Tellus (1990), *42A*, 78–91

Model simulations of an intense meso-β scale cyclone The role of condensation parameterization

By JÓN EGILL KRISTJÁNSSON, *Section of Meteorology, University of Bergen, Allégaten 70, N-5007 Bergen, Norway*

(Manuscript received 7 November 1988; in final form 6 June 1989)

ABSTRACT

On 23 July 1985, an unusual mesoscale storm struck the Baltic Sea coast of Sweden. Locally, more than 50 mm of precipitation fell in 12 h and mean winds exceeding 25 m s^{-1} were recorded. The failure of operational models to predict this storm, as well as the damage it caused (2 people were killed), raised important questions. What physical process caused this rare event? Could it be predicted with existing data, and if so, how? Diagnostic studies reveal the following features. The development took place in a very humid air mass, which possessed weak conditional stability. The synoptic-scale environment provided large relative vorticity, which helped to spin up the mesoscale vortex. Calculations show significant adiabatic forcing initially, but then latent heat release takes over as the main driving mechanism. Numerical simulations of this storm show that it can be successfully simulated with a regional model, provided that condensation and latent heat release are treated in a consistent manner. This is demonstrated, e.g., by comparing latent heating distributions in 2 different condensation schemes. The simulations, furthermore, demonstrate the crucial role of good humidity data for this type of simulations.

1. Introduction

In recent years, a steady progress has taken place in regional scale modelling, see, e.g., Anthes (1989). As a result of this progress, a growing number of studies have utilized these so-called limited area models (LAMs) to successfully simulate the structure and development of explosive cyclone developments, e.g., Anthes et al. (1983), Kuo and Reed (1988), Gyakum and Barker (1988). Improvements in the parameterization of physical processes and in model resolution have also made it increasingly feasible to simulate mesoscale weather systems. These include polar lows, e.g., Sardie and Warner (1985), Grønås et al. (1987) as well as coastal cyclogenesis, e.g., Leslie et al. (1987) and continental convective complexes, e.g., Zhang and Fritsch (1986).

Latent heating often plays a paramount role as an energy source in mesoscale weather systems, although its importance compared to other forcing mechanisms may vary. For instance, in the case of polar lows, it has been argued that some of these systems are mainly driven by latent heating, cf. e.g., Økland (1987), Emanuel and Rotunno (1989), while other cases and other authors point more in the direction of baroclinic forcing, e.g., Reed and Duncan (1987).

In this study, we shall present several LAM simulations of a rare mesoscale event that took place in the Baltic Sea in July 1985. Through these simulations we shall seek to answer the following questions. What role does the latent heating play for this mesocyclone? How important are details in the physical parameterizations for the quality of the simulation? How sensitive are the simulations to variations in initial data and surface parameters?

An important difference from other model studies of small-scale cyclones is that the emphasis here will be on the significance of consistency in the treatment of condensation processes. In particular, comparisons will be made between the

consistent cloud parameterization scheme of Sundqvist (1988), and a more simple, diagnostic scheme. The first of these has already been used successfully in the simulation of the life cycle and structure of an intense synoptic scale cyclone in Sundqvist et al. (1989). In the case studied here, it is shown that the introduction of this scheme gives a far more realistic horizontal and vertical distribution of latent heat release, clouds and precipitation than the diagnostic scheme. This, in turn leads to major improvements in the simulation of pressure patterns and winds. It should be kept in mind that many of the above mentioned model studies have cloud parameterization approaches similar to the diagnostic scheme that is used as a reference in this study.

2. Model and data treatment

For the simulations and some of the diagnostics in this study we have modified the LAM of the Norwegian Meteorological Institute, described in Grønås et al. (1987). (In the sequel the modified version will be referred to as UBVERS, while the unmodified version will be termed MIVERS.) This model has a horizontal grid distance of approximately 50 km and the number of grid points is 61 × 49. In the vertical direction there are 10 σ-levels, with the highest level fixed at 200 hPa.

The modifications of the model consist of a more sophisticated treatment of condensation and clouds, in accordance with Sundqvist (1988), and a modified parameterization of vertical diffusion. These modifications are described in detail in Sundqvist et al. (1989). The most important improvement is that humidity, condensation, latent heat release and cloud formation and dissipation are now treated in a consistent way. This is accomplished by combining the continuity equations for humidity and cloud water, which is a prognostic variable, and the temperature tendency equation, in such a way that they form a closed set of equations.

In the case of stratiform clouds, cloud formation is assumed to begin as soon as the grid box relative humidity exceeds U_0, where U_0 is a function of cloudiness and surface type, but lies in the range 0.75–1.0. This means that stratiform condensation is treated as a sub-grid scale process in UBVERS. In MIVERS, on the other hand, a simple diagnostic scheme is used for computations of stratiform condensation and precipitation, see Nordeng (1986). The MIVERS scheme is identical to the one described by Manabe et al. (1965) and Haltiner and Williams (1980, pp. 313–314), except for the inclusion of cloud water as a diagnostic quantity, which determines the rate of precipitation.

For convective condensation, UBVERS uses a Kuo (1965, 1974) scheme, modified to include cloud water as a prognostic variable, cf. Sundqvist (1988). MIVERS, on the other hand, uses a Kuo-type scheme with a different formulation. For instance, in UBVERS, convection is only allowed if a surface parcel of air is unstable after being lifted to saturation (LCL). In MIVERS, on the other hand, convection can be initiated at any level in the air column, provided there is instability at that level and a convergence of moisture, $C_m > 0$. A further, important, difference between the schemes of the two versions is that the contribution from surface fluxes to the term C_m is neglected in the MIVERS. This may possibly be an important deficiency. Finally, MIVERS does not apply the Kuo scheme when the column above LCL is supersaturated. Instead, a convective adjustment scheme, similar to the one designed by Manabe et al. (1965) is applied in these points.

The vertical eddy diffusion schemes in UBVERS and MIVERS are similar to the ECMWF scheme, described by Tiedtke et al. (1979). In UBVERS, the turbulent transport is enhanced in clouds. For more details, see Sundqvist et al. (1989). It should be mentioned that neither model version includes horizontal diffusion.

Data sets for the model are processed in the assimilation scheme at the Norwegian Meteorological Institute, described in Grønås and Midtbø (1987). Boundary values are incorporated every 6 h. In the present case, analyses have been used at the boundaries. Since cloud water is not included in the assimilation and analysis scheme, all the runs in this study start out with zero cloud water in all points. Also boundary values have zero cloud water. For this reason, some spin-up time has to be expected. In Sundqvist et al. (1989), the spin-up time was estimated to be of the order 7–8 h, while an analogous estimate here yields approximately 6 h.

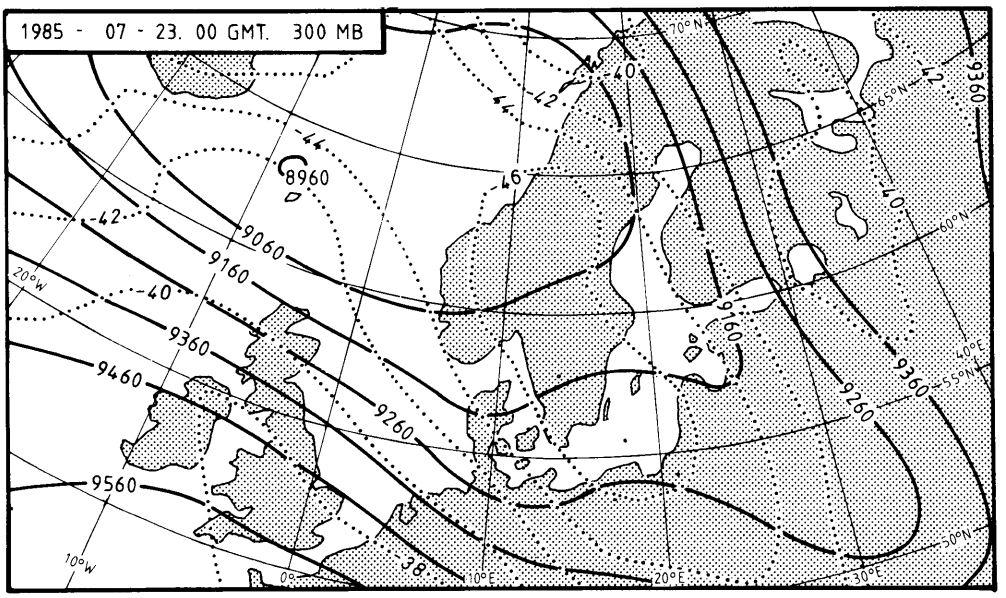

Fig. 1. Subjectively analyzed 300 hPa geopotential heights (solid, 100 m intervals) and temperature (dotted, 2°C intervals) at 00 GMT 23 July 1985.

3. Diagnosis of the synoptic development

3.1. Synoptic background

On 22–23 July 1985, the weather situation over Northern Europe was characterized by a deep upper low just east of Iceland, and an associated upper trough extending south-eastwards towards the Baltic Sea (Fig. 1). In connection with this trough, the upper air temperatures were well below average in a zone covering Southern Scandinavia and Poland, extending into the Soviet Union.

At the surface, a 1003 hPa low was located over Scotland at 12 GMT 22 July. During the next 12 h, this low moved eastwards into Denmark, deepening 1 hPa as it entered the occluding phase. It was in connection with this apparently mature cyclone that an intense meso-β scale low developed in the early hours of 23 July. We shall now have a closer look at the conditions

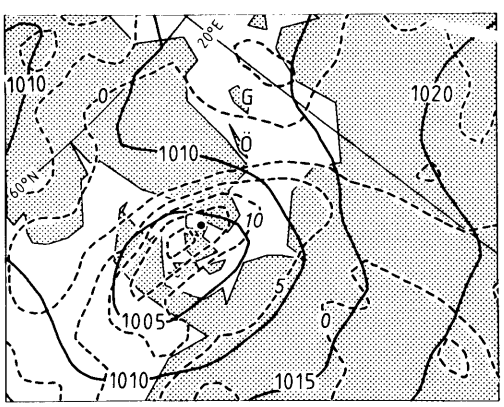

Fig. 2. Objective analysis of sea-level pressure (solid, every 5 hPa) and relative vorticity at σ_7 ($\approx$840 hPa; dashed, units of 10^{-5} s^{-1}) at 00 GMT 23 July. Some geographical locations referred to in the text are indicated, C: Copenhagen, Ö: Öland, G: Gotland.

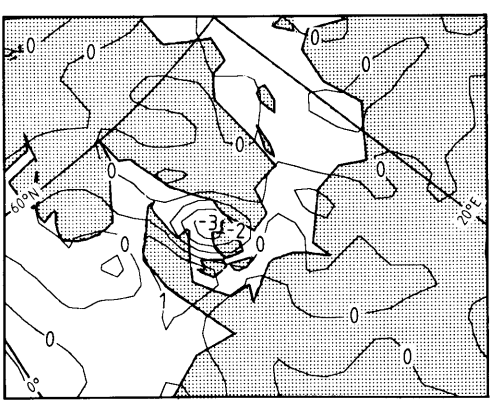

Fig. 3. Q-vector divergence (units of 10^{-16} m^{-1} s^{-3}) at 700 hPa at 00 GMT 23 July.

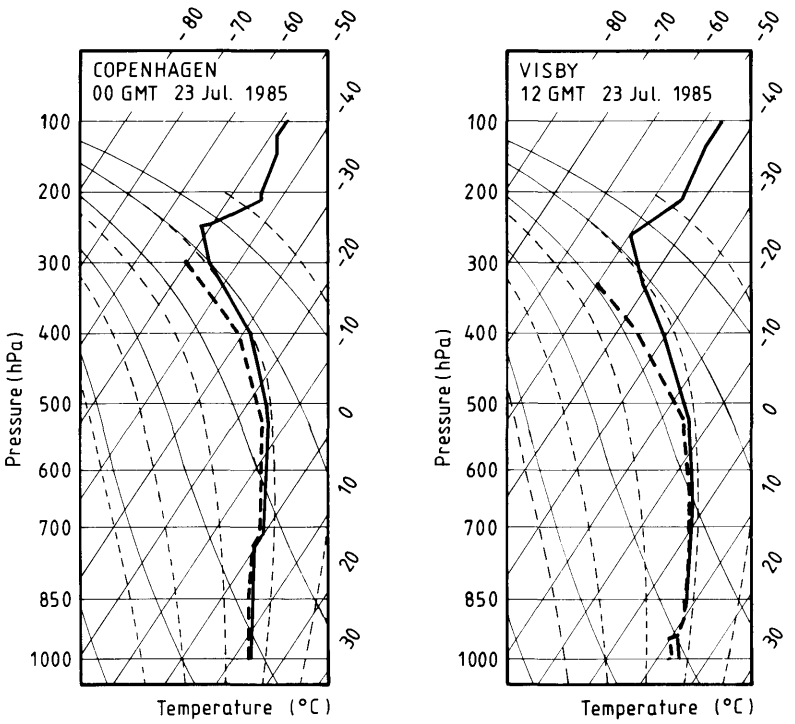

Fig. 4. Radiosonde soundings from Copenhagen, at 00 GMT 23 July and Visby, Gotland, at 12 GMT 23 July. Heavy solid line is temperature curve, heavy dashed line dew point temperature.

at 00 GMT 23 July, which is also the starting time for most of the simulations in Section 4.

Fig. 2 shows the sea level pressure, together with relative vorticity at approximately 840 hPa at 00 GMT 23 July. We note that there is a rather strong vorticity maximum of more than $2 \cdot 10^{-4}$ s^{-1} at the center of the cyclone over Denmark. It has been shown by Økland (1987), with a linear CISK model, how a synoptic-scale, mature cyclone with vorticity equal to $2f$ (f being the Coriolis-parameter) can yield a favourable environment for the formation of convectively driven polar lows. A case study of a mesoscale Mediterranean low by Rasmussen and Zick (1987) seems to support this theory. It seems plausible that the large-scale vortex with its large vorticity may have played a similar role in this case (see also discussion in Subsection 4.2).

To obtain a quantitative measure of the forcing of vertical motion at 00 GMT 23 July, we can make use of the Q-vector form of the ω-equation (ω being the vertical velocity in pressure coordinates), defined in Hoskins and Pedder (1980). Note that the diabatic term, which is neglected in that paper has been added here:

$$S\nabla^2\omega + f^2\frac{\partial^2\omega}{\partial p^2} = -2\frac{R}{p}\left(\frac{p}{p_0}\right)^{R/C_v}\nabla\cdot\boldsymbol{Q} - \frac{R}{p}\nabla^2 H, \tag{3.1}$$

where Q is defined by the expression

$$Q \equiv \frac{\mathrm{d}_g}{\mathrm{d}t}\nabla\theta, \tag{3.2}$$

θ being potential temperature and the subscript g

Fig. 5. (a)–(d) Subjectively analyzed sea-level pressure (hPa) and fronts at 09, 12, 15 and 18 GMT 23 July, respectively. Dashed lines are pressure tendencies in hPa/(3 h). (e)–(h) Model-predicted sea-level pressure (hPa) from control run at same times as in (a)–(d).

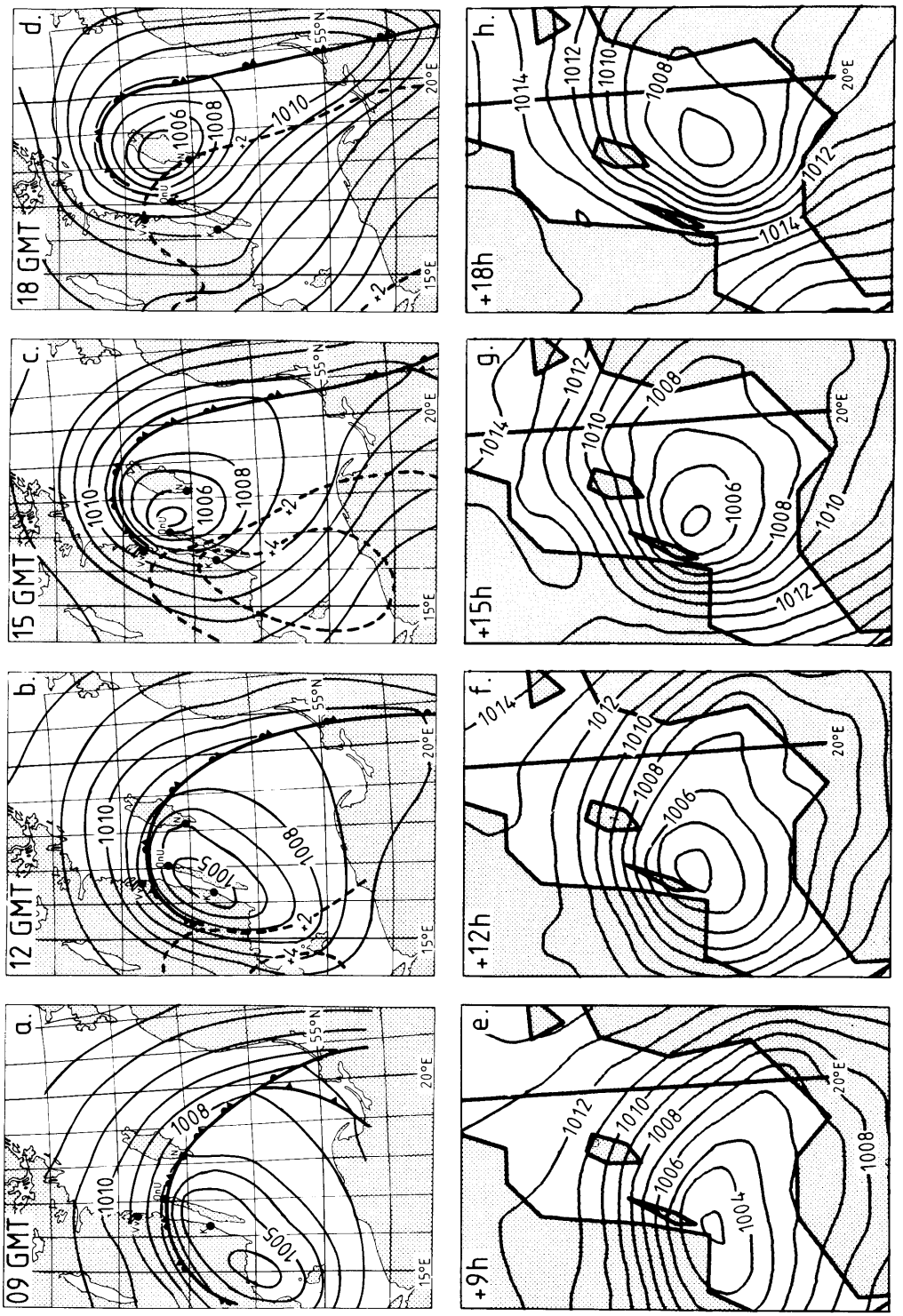
a.
09 GMT
b.
12 GMT
c.
15 GMT
d.
18 GMT
e.
+9h
f.
+12h
g.
+15h
h.
+18h
1005
1006
1008
1010
1012
1014
+2
+4
55°N
15°E
20°E

meaning geostrophic. In (3.1), S is the static stability parameter

$$S = -\frac{\alpha}{\theta}\frac{\partial \theta}{\partial p}, \tag{3.3}$$

where α denotes specific volume and p pressure; R is the gas constant for dry air, $p_0 = 1000$ hPa, C_p specific heat of dry air at constant pressure and H is the diabatic heating rate in K s^{-1}.

The contribution from the first term (adiabatic) on the right hand side in (3.1) has been computed from the analysis on the model grid. Fig. 3 shows the results obtained at 700 hPa. As we see, there is a forcing of rising motion ahead of the cyclone and sinking motion in its rear, corresponding to a conversion of available potential energy to kinetic energy.

An estimate of the contribution from latent heating can be readily obtained from the model. Due to the spin-up time of the cloud parameters in the model (cf. end of Section 2), I have used output from the run starting at 12 GMT 22 July, i.e., 12 h before the time in question. The results (not shown) show a positive maximum of more than $3 \cdot 10^{-4}$ K s^{-1} near the cyclone center. The resulting forcing in (3.1) is about twice as large as from the adiabatic term. Also, an even larger heating maximum of $1.0 \cdot 10^{-3}$ K s^{-1} is found in association with the frontal systems. Similar calculations at later times (e.g., Fig. 9) also indicate that the forcing from latent heating is larger than that from adiabatic effects.

At 00 GMT 23 July, heavy rain was reported at Copenhagen and a pressure fall of 5.4 hPa during the previous 3 h. The sounding from Copenhagen (Fig. 4) shows a very humid atmosphere from the surface all the way up to the tropopause, which was at 250 hPa. Conditional stability was weak, except for an inversion near 700 hPa. This means that the response to forcing in eq. (3.1) will be large, since S is small (with θ replaced by θ_e). It is interesting to note how these conditions are maintained at the center of the cyclone, cf. the sounding from Visby, on the west coast of Gotland (G in Fig. 2), 12 h later, Fig. 4.

3.2. *The Baltic Sea mesoscale storm*

Fig. 5 shows the evolution of the surface cyclone on 23 July, as compared to a model simulation with UBVERS, starting from 00 GMT 23 July. Looking first at the subjective analyses (Fig. 5a–d) and observations (Fig. 6) we note that at 09 GMT, there is widespread moderate or heavy precipitation and poor visibility in southern Sweden and the Baltic Sea islands of Öland and Gotland (see Fig. 2 for location), in connection with the frontal system. The cyclone center has started to broaden or split as a new development has started over the northern part of Öland (see, e.g., wind and pressure changes at Kalmar in Fig. 6). The pressure falls ahead of the cyclone are weaker now than at 00 GMT, but more significantly, there are large pressure rises in the rear of the cyclone at the same time as the central pressure remains unchanged (cf. Fig. 6). Thus, the cyclone does not intensify through a reduction in central pressure, as is characteristic of most developing cyclones, but instead through a reduction in scale. Note, for instance how the 1010 and 1005 hPa isobars come tighter together between 09 GMT and 15 GMT (Fig. 5). How can this intensification be explained in terms of physical and dynamical processes?

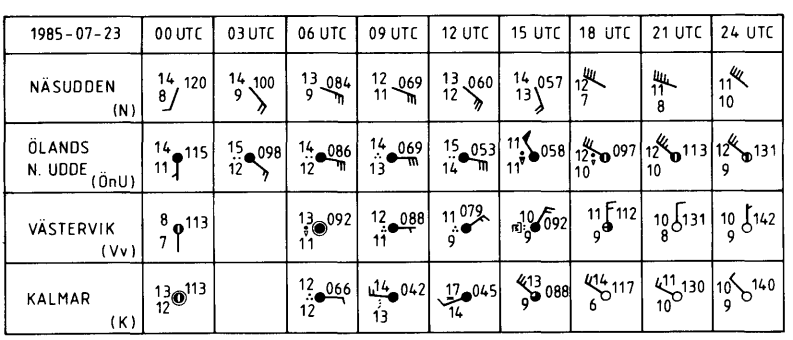

Fig. 6. Significant weather, cloudiness, temperatures and pressure at four synoptic stations (see Fig. 5a–d and Fig. 8a). Standard WMO notation is used.

As has been shown by, e.g., Sawyer (1956) and Eliassen (1959), latent heat release, in connection with frontal upgliding can give rise to enhanced vertical motion and a sharpening of gradients. Since latent heat release is very strong in this case, as discussed in Subsection 3.1, it will be suggested that this is the most important process in the ensuing development. This hypothesis will be further supported in the next section.

A noticeable feature at 12 GMT (Fig. 6), is the large temperature difference across the front. Thus, near the cyclone center, at Kalmar (K in Fig. 5b), the temperature is 17°C, with a dewpoint of 14°C, while just 100 km away, in the cold northeasterly flow, at Västervik (Vv in Fig. 5b), the temperature and dewpoint are 11°C and 9°C, respectively. The concentration of warm, humid air in the core of the cyclone is well illustrated by the 850 hPa isotherms in Fig. 7.

The 15 GMT observations indicate a further strengthening of the winds in the rear of the cyclone (Fig. 6). Most noticeable is the 24 m s^{-1} wind at the northern tip of Öland (ÖnU in Fig. 5a–d), where an even higher recording of 27.5 m s^{-1} occurred between 15 and 16 GMT. Näsudden (N in Fig. 5a–d) at the southern tip of Gotland recorded an increase in wind speed from 6.5 m s^{-1} at 16 GMT to 20.5 m s^{-1} at 18 GMT as the wind veered from a southerly direction to WNW-erly (Fig. 6). We also note from Fig. 6 that thunderstorms occurred at Västervik (Vv) between 14 and 15 GMT. The radiosonde sounding from Visby, Gotland at 12 GMT 23 July (Fig. 4), shows an atmosphere slightly stable to moist-adiabatic ascent, except for a more stable layer in the lowest 100 hPa. Since this layer does not seem to permit deep convection, it indicates that the thunderstorm activity mentioned above was probably confined to a small region.

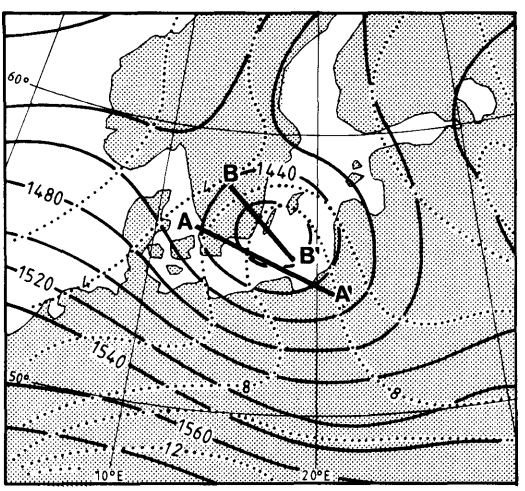

Fig. 7. Subjectively analyzed 850 hPa geopotential heights (solid, 20 m intervals) and temperature (dotted, 2°C intervals) at 12 GMT 23 July. The locations of cross-sections are indicated by line segments AA′ and BB′.

4. Simulations with imposed changes in model or data

4.1. Results from control simulation

The UBVERS simulation starting from 00 GMT 23 July will hereafter be referred to as the control run. Fig. 5e–h shows the sea level pressure prediction from this simulation. Comparing with the subjective analysis, we note a very close similarity as far as pressure gradients and depth of the low are concerned. However, the position of the surface cyclone is slightly in error, the model cyclone being displaced approximately 50 km southwards, compared to the verifying analyses at 15 GMT and later.

The precipitation from this run for the period 06 GMT–18 GMT is shown in Fig. 8, together with a verifying analysis. Again, the quality of the forecast is satisfactory. Not less significant than the successful predictions of pressure fields and precipitation distribution is the fact that the cloud distribution and frontal structure are realistically reproduced in this simulation. For instance, Fig. 9, which shows the instantaneous latent heating rate, exhibits a frontal-like structure, similar to the observed front (Figs. 5b, 10), a feature not seen in the MIVERS run (not shown).

During the intense phase of the cyclone, cross-sections of latent heating rate (Fig. 11) show a narrow and strong maximum in the region above the maximum surface winds (ÖnU in Fig. 6). The ageostrophic motion is shown in the same cross-section (computed by subtracting the geostrophic wind from the predicted wind). According to this figure, there is a zone of approximate

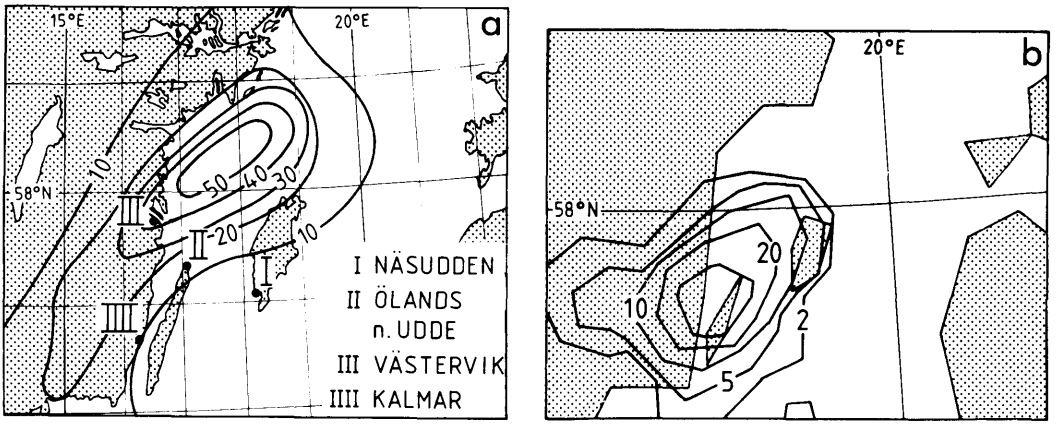

Fig. 8. (a) Analysis of observed 12-h precipitation in the period 06–18 GMT 23 July. Lines are drawn for every 10 mm. Synoptic stations (Fig. 6) are indicated by I–IIII. (b) Predicted 12-h precipitation in the period 06–18 GMT 23 July; control run. Lines are drawn for 2, 5, 10, 20 and 40 mm.

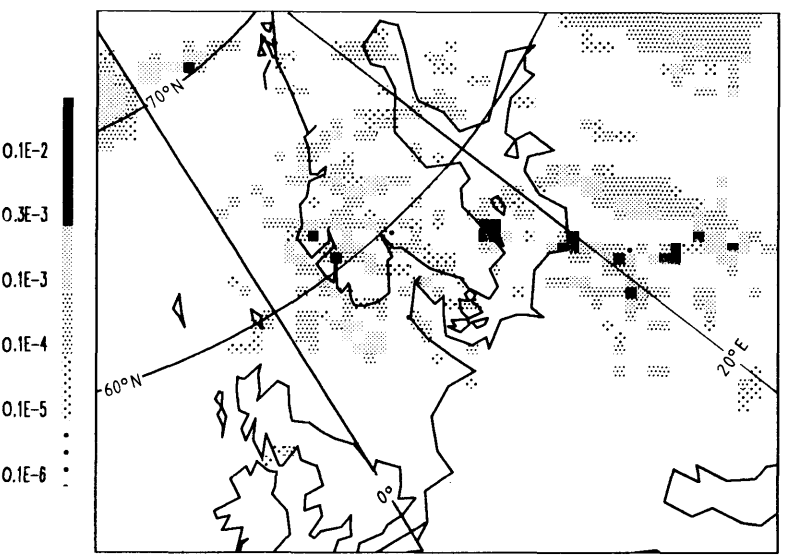

Fig. 9. Latent heating rate at σ_6 ($\approx$740 hPa) at 12 GMT 23 July (control run). Shading is explained by scale on the left. Units: K s^{-1}.

width 100 km, with strong rising motion, and an associated convergence near the surface. The spatial dimension of this region of intense activity seems to correspond well with observations (Figs. 5b, 6). Similarly, the "low-level-jet" to the west and northwest of the cyclone corresponds well to observed wind maxima.

The possible role of symmetric instability and slantwise convection in the cyclone intensification has been considered. The theory for symmetric instability was described in Eliassen and Kleinschmidt (1957), but has recently gained renewed interest due to the works of Bennetts and Hoskins (1979) and Emanuel (1983, 1985), in particular. Fig. 12 shows lines of constant absolute momentum M, and equivalent potential temperature θ_e at 12 GMT in the cross-section BB′ (cf. Fig. 7) at 12 GMT. According to the theory,

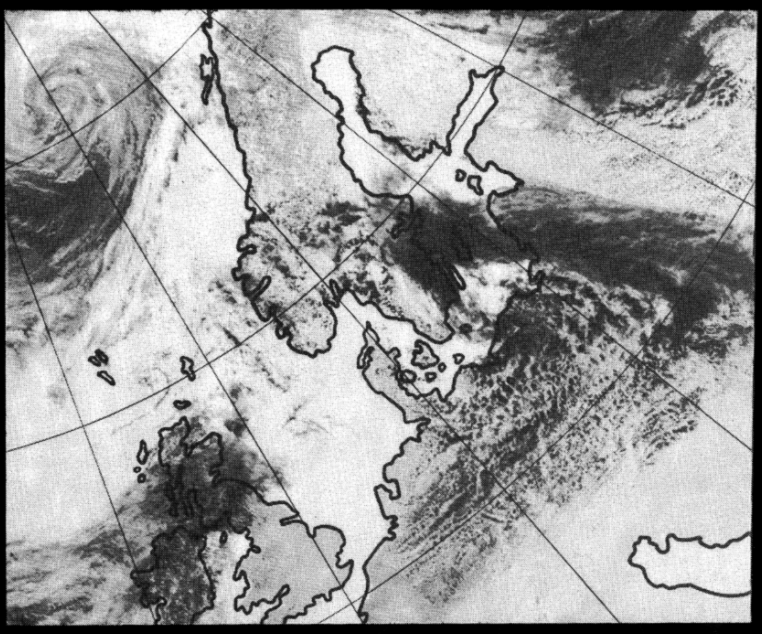

Fig. 10. NOAA-9 satellite picture in the visible range, taken between 10:57 GMT and 14:32 GMT 23 July. (Courtesy of Institut für Meteorologie, Freie Universität, Berlin.)

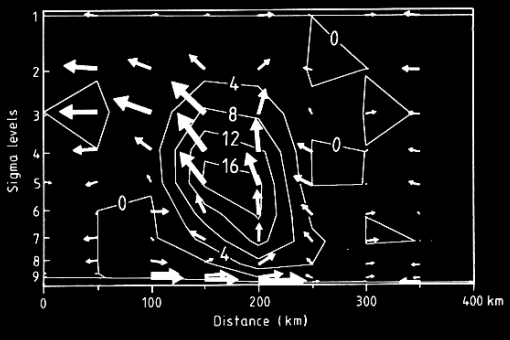

Fig. 11. Latent heating rate (units of 10^{-4} K s^{-1}) and ageostrophic winds, in cross-section BB′ (cf. Fig. 7) at 12 GMT 23 July (control run). Scales for horizontal and vertical components are as follows: Horizontal: an arrow of length 1 grid-distance (50 km) corresponds to 14 m s^{-1} wind speed. Vertical: an arrow of height delta-sigma (distance between consecutive sigma-levels) corresponds to approximately 3 Pa s^{-1}.

the atmosphere will be symmetrically unstable where the lines of constant θ_e have a tilt that is greater than the tilt of the M-lines, with respect to the x-axis. Additionally, we have to require that the air be saturated for instability to occur. As we see from Fig. 12, there is a very weak symmetric stability in most of the shaded region. In fact, above σ_7, there is a large region which is unstable to symmetric perturbations of saturated air. Furthermore, this region coincides with the region of maximum ascent (slantwise) in Fig. 11.

It has to be kept in mind that the evaluation of symmetric instability presented above is based on model output data, which have been subjected to interpolation and smoothing. Also, the theory is purely two-dimensional, and therefore requires that there be no net force in the direction perpendicular to the plane. This seems to be reasonably well satisfied here, since the ageostrophic tangential velocities are rather small above the boundary layer, Fig. 11. It remains something of an open question to which extent the model may simulate the effects of slantwise convection, without an explicit parameterization of it (see, e.g., Thorpe (1986), Nordeng (1987)).

For these reasons, I feel that it is hardly possible to draw any far-reaching conclusions on the possible role of slantwise convection at this stage. However, the above results suggest that this process could have taken place at 12 GMT 23 July, precisely at the time when the low was entering its most intense phase. A similar result

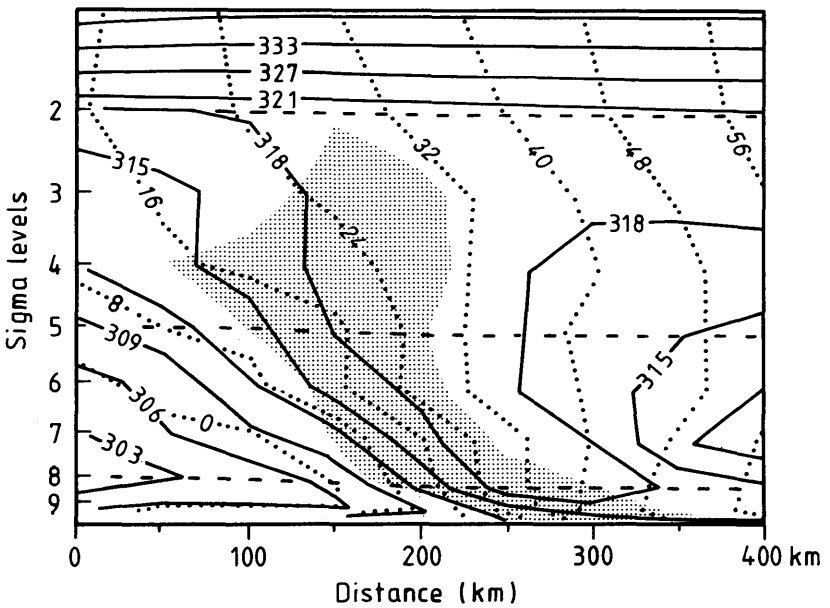

Fig. 12. Equivalent potential temperature (solid, every 3 K) and absolute momentum (dotted, every 4 m s^{-1}) in cross-section BB′ (cf. Fig. 7), at 12 GMT 23 July (control run). Shaded area for relative humidity 100%.

was obtained by Sanders and Bosart (1985), in their study of an intense coastal snowstorm. It should be mentioned that the corresponding cross-sections of M and θ_e at +6 h, +9 h and +18 h do not exhibit the features discussed here, while the cross-section from +15 h is similar to Fig. 12.

4.2. *Simulation with diagnostic condensation scheme (MIVERS)*

Here, we shall present results from the model simulation with the original version of the model (MIVERS). As discussed in Section 2, it differs from the UBVERS mainly in the parameterization of condensation and clouds, but also in the parameterization of vertical eddy diffusion.

Comparing the results from this run with the observations and the control run, it turns out that the MIVERS simulation is clearly inferior. While the cyclone follows almost the same track as in the control run, the central pressure is several hPa higher (Table 1). As a result, the pressure gradient is far too weak, so the strong winds near Öland and Gotland are missing. Similarly, the distribution and amount of precipitation fail to show the pronounced maxima that were observed, and realistically captured in the control run. The same failure was present in other operational models at the time.

To isolate the effects of the two modifications mentioned above, the model has been rerun with the MIVERS vertical diffusion scheme and the UBVERS condensation scheme. The central pressure obtained is shown in Table 1 ("Old diffusion"). As we see, the cyclone was not quite as deep in this run as the control, but the pressure gradient and amount of precipitation are both very similar to the control run. Thus, the main difference between the UBVERS and the MIVERS results stems form the different treatment of condensation and clouds.

Referring to the discussion in Subsection 3.1, on the role of vorticity, it is interesting to note that the vorticity in the control run increased from approximately 2.0f at 06 GMT to 3.5f at 15 GMT, while the corresponding vorticity in MIVERS at 15 GMT was only 2.0f.

Fig. 13 shows the heating rates from condensation in the MIVERS run, compared to the same quantity in the control run at +6 h, i.e., at the time when the intensification of the mesocyclone starts. Even though the vertically integrated heating rates in the two cases are not very different, there is a very significant difference in

Table 1. *Central pressure in Baltic Sea cyclone on 23 July 1985 for different simulation runs and observed. (Units: hPa)*

	00 GMT	06 GMT	09 GMT	12 GMT	15 GMT	18 GMT	21 GMT
observed	1002	1003	1004	1004	1005	1005	1006
control run	1002	1003	1003	1004	1005	1007	1009
old diffusion	1002	1004	1004	1004	1005	1008	1009
MIVERS	1002	1005	1006	1008	1009	1011	1012
no convective heating	1002	1003	1003	1005	1006	1007	1009
no stratiform heating	1002	1005	1007	1009	1011	1012	1012
reduced z_0	1002	1003	1002	1003	1004	1006	
reduced initial hum.	1002	1005	1007	1009	1011	1012	1012
initial hum. = 100%	1002	1003	1003	1004	1004	1006	1007
start 00 GMT 22 July	1005	1003	1003	1005			
start 12 GMT 22 July	998	1001	1003	1004	1005	1006	1007
start 18 GMT 22 July	999	996	999	1001	1003	1004	

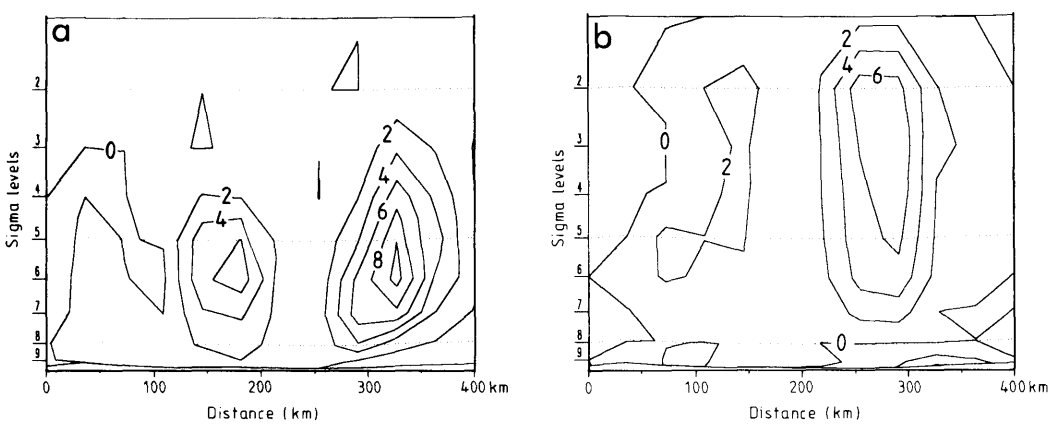

Fig. 13. Latent heating rate in cross-section AA′ (cf. Fig. 7) at 06 GMT 23 July (units of 10^{-4} K s^{-1}). (a) UBVERS, +6 h (control run), (b) MIVERS, +6 h.

the vertical distribution of this heating. Whereas the heating in the MIVERS run peaks at sigma level 2 (corresponding to ≈350 hPa), the maximum heating in the UBVERS run is at σ_6 (≈740 hPa), with practically no contribution from the top three levels (≈250–450 hPa). It is well known that the level at which a heat source is placed in the atmosphere makes a decisive difference for the response that follows. This has been shown in numerical model studies (e.g., Anthes and Keyser (1979), Gyakum (1983)) and theoretical studies (e.g., Bratseth (1985)). It is also compatible with the potential vorticity viewpoint of Hoskins and Berrisford (1988). In short, the lower the level at which the latent heat is released, the stronger will the response be, in terms of low-level horizontal convergence and rising motion.

There appear to be 3 main reasons for the difference in vertical distribution of the latent heating in the two cases. Firstly, in UBVERS the condensation is treated as stratiform in most of the region shown in Fig. 13, while MIVERS treats it as convective. This is due to the inversion in the lowest 1–2 model levels (cf. Fig. 4), which prevents convection in UBVERS, but not in MIVERS (cf. Section 2). Since the purpose of the convective treatment is precisely to distribute the heat vertically, while the stratiform scheme releases it in situ, one would expect this distinc-

tion to be important. It should be noted, however, that with a temperature and humidity distribution as shown in Fig. 4, the redistribution of heat and moisture in the Kuo-scheme should have little effect. Secondly, the use of a moist adiabatic adjustment scheme for saturated, convective points in MIVERS (cf. Section 2) may have affected the stratification near the cyclone center, thus leading to a different evolution. Thirdly, there is little doubt that the higher degree of consistency in the condensation parameterization in UBVERS, as compared to MIVERS, will contribute to a better simulation in the first, but this effect is difficult to quantify.

4.3. Simulations without latent heating from stratiform or convective condensation

To study the impact of latent heating on the quality of the simulations, two runs have been conducted, where the temperature tendencies from stratiform and convective condensation (and evaporation), respectively, have been set equal to zero at all times. In the first case the effect was drastic, since the central pressure of the low was 6 hPa too high, see Table 1. Consequently, the winds and precipitation were grossly in error in this run. Neglecting the convective heating, on the other hand, did not have a great impact (Table 1). The relative importance of stratiform versus convective heating is not surprising, since most of the condensation near the cyclone center is treated as stratiform in UBVERS (cf. Subsection 4.2).

4.4. Simulations with imposed changes in surface conditions

To test the possible role of frictional convergence, due to larger friction over land than over sea, on the cyclone development, simulations have been made where the roughness length z_0 has been set equal to 10^{-4} m over land, instead of 0.3 m in the control run. It turned out (Table 1) that the cyclone became 1–2 hPa deeper than in the control run, with a corresponding increase in wind speed, whereas the precipitation pattern remained almost unchanged. This seems to indicate that the friction in this case mainly acts as a dissipating effect, rather than acting to enhance the low level convergence of moisture.

4.5. Simulations with different initial conditions

To get a rough idea of the sensitivity to initial data, some runs have been made where the initial humidity has been altered. In one of these experiments, the initial humidity field was multiplied by a factor 0.5 in the lowest 5 sigma-levels (below 700 hPa). The resulting cyclone development was several hPa too weak (Table 1), yielding far too weak winds and far too light precipitation compared to observations. This indicates that the lower-level humidity available for condensation and latent heat release is crucial for the development of an intense vortex.

Setting the initial relative humidity equal to 100% at all points turned out to give a cyclone which was 1 hPa deeper than in the control run (see Table 1). However, the cyclone was less intense than in the control run, in the sense that the winds were weaker and precipitation was less concentrated. Convective precipitation was very widespread and heavy in many places. Thus, we see that it is not only the amount of humidity that is important for the type of response we get, but equally important is the horizontal distribution of humidity. Particularly important is the concentration of humidity in certain places that are favourable for cyclone deepening through condensation and latent heat release. This underlines what was said in Subsection 4.2, on how the UBVERS gives a more concentrated latent heat release than MIVERS. It also relates to the discussion in Subsection 3.1 on the important role of the synoptic scale in providing a favourable environment for the formation of intense mesoscale vortices.

To test the ability of the UBVERS to give an early forecast warning of the mesoscale development that took place on 23 July, the model has been rerun starting at 00, 12 and 18 GMT 22 July, respectively. The results (cf. Table 1) show that the 00 GMT and 12 GMT runs give an early indication of a secondary low center near Öland at 12 and 15 GMT 23 July, with a strong pressure gradient in the rear. The precipitation indicated by both these runs is considerably weaker than what was observed, and the wind speed is underestimated. However, both simulations indicate that the processes which created this mesoscale cyclone were reasonably predictable on the basis of existing data, at least $1\frac{1}{2}$ days in advance.

The simulation from 18 GMT is an exception.

In this case, the cyclone deepens far more in the southern part of the Baltic Sea, resulting in a deep, broad cyclone shifted 100–200 km southeastwards compared to the control run. A careful look at the humidity field shows considerable differences near the cyclone center compared to the other runs. It should be kept in mind that no radiosonde data are available as input in the data assimilation at 18 GMT, as opposed to what is the case at 00 and 12 GMT. Thus, the humidity data are likely to be less reliable in this case. The result again underlines the crucial importance of the initial humidity distribution, for obtaining a good simulation.

5. Summary and conclusions

In this study, several simulation experiments of an intense mesoscale low have been carried out with the aid of a LAM with 50 km horizontal resolution. The emphasis has been on the effect of variations in the physical parameterizations and initial data. In particular, the effect of introducing a sophisticated treatment of condensation and clouds, following Sundqvist (1988), has been closely investigated. Also, diagnostic calculations have been made, to establish a comprehensive picture of the mesoscale development.

The main findings of this study are the following.

- It is suggested that the mesoscale development was initiated through a combination of large-scale vorticity helping to spin up the mesocyclone, and the presence of very humid air, which possessed weak conditional stability. Once this air was forced to rise through synoptic-scale forcing, the system became self-sustained through a feedback between strong latent heat release and low-level convergence.
- Contrary to earlier belief, it has been shown that this event can be successfully simulated with existing model resolution and data. However, the simulations are crucially dependent on the treatment of condensation and latent heat release. Using the scheme of Sundqvist (1988), precipitation and cloud distribution, as well as pressure patterns, are realistically reproduced. The simpler diagnostic scheme considered, is found to release the latent heat at a much higher level, yielding a much weaker development than observed.
- Variations in the treatment of surface friction, vertical diffusion and surface humidity turned out to be of minor importance for the quality of the simulations.
- The simulations show a great sensitivity to initial humidity. It has been shown that the distribution of the initial humidity is at least as important as the amount of it. No cyclone deepening occurs when low-level initial humidity is reduced by 50%.

6. Acknowledgements

The author is indebted to Professor Hilding Sundqvist for stimulating discussions and comments on the manuscript. Many thanks to Karl-Göran Karlsson, SMHI, Sweden, for helpful suggestions, and for providing analysis material. Fritz Larsson is thanked for supplying useful material, Frank Cleveland for preparing the figures and Rita Moi for hand-analyzing surface charts. Computer runs were done free of charge on the IBM 3090/200 at Bergen Scientific Center. Finally, advice regarding computer runs and graphics, by Anstein Foss and Dr. Thor Erik Nordeng at the Norwegian Met. Inst., and by Ronny H. Andersen at IBM/BSC is gratefully acknowledged.

REFERENCES

Anthes, R. A. 1989. Advances in the understanding and prediction of cyclone development with limited-area fine-mesh models. In: *Palmén Memorial Symposium on Extratropical Cyclones*. Lead papers. American Meteorological Society, in press.

Anthes, R. A. and Keyser, D. 1979. Tests of a fine-mesh model over Europe and the United States. *Mon. Wea. Rev. 107*, 963–984.

Anthes, R. A., Kuo, Y.-H. and Gyakum, J. R. 1983. Numerical simulations of a case of explosive marine cyclogenesis. *Mon. Wea. Rev. 111*, 1174–1188.

Bennetts, D. A. and Hoskins, B. J. 1979. Conditional symmetric instability—a possible explanation for frontal rainbands. *Quart. J. R. Met. Soc. 105*, 945–962.

Bratseth, A. 1985. A note on CISK in polar air masses. *Tellus 37A*, 403–406.

Eliassen, A. 1959. On the formation of fronts in the atmosphere. In: *The Rossby Memorial Volume* (ed. B. Bolin). New York: Rockefeller Institute & Oxford University, 277–287.

Eliassen, A. and Kleinschmidt, E. 1957. *Dynamic*

Meteorology, Handb. Phys. 48. Berlin: Springer Verlag, 71–72.

Emanuel, K. A. 1983. The Lagrangian parcel dynamics of moist symmetric instability. *J. Atmos. Sci. 40*, 2368–2376.

Emanuel, K. A. 1985. Frontal circulations in the presence of small moist symmetric stability. *J. Atmos. Sci. 42*, 1062–1071.

Emanuel, K. A. and Rotunno, R. 1989. Polar lows as arctic hurricanes. *Tellus 41A*, 1–17.

Grønås, S. and Midtbø, K. H. 1987. Four-dimensional data assimilation at the Norwegian Meteorological Institute. In: *Short- and medium-range numerical weather prediction* (ed. T. Matsuno). Collection of papers presented at the WMO/IUGG NWP symposium, Tokyo, 4–8 August 1986, 61–74.

Grønås, S., Foss, A. and Lystad, M. 1987. Numerical simulations of polar lows in the Norwegian Sea. *Tellus 39A*, 334–353.

Gyakum, J. R. 1983. On the evolution of the QE II storm. II: Dynamic and thermodynamic structure. *Mon. Wea. Rev. 111*, 1156–1173.

Gyakum, J. R. and Barker, E. S. 1988. A case study of explosive subsynoptic-scale cyclogenesis. *Mon. Wea. Rev. 116*, 2225–2253.

Haltiner, G. J. and Williams, R. T. 1980. *Numerical prediction and dynamic meteorology.* Chichester: Wiley, 477 pp.

Hoskins, B. J. and Pedder, M. A. 1980. The diagnosis of middle latitude synoptic development. *Quart. J. R. Met. Soc. 106*, 707–720.

Hoskins, B. J. and Berrisford, P. 1988. A potential vorticity perspective of the storm of 15–16 October 1987. *Weather 43*, 122–129.

Kuo, H. L. 1965. On formation and intensification of tropical cyclones through latent heat release by cumulus convection. *J. Atmos. Sci. 22*, 40–63.

Kuo, H. L. 1974. Further studies of the parameterization of the influence of cumulus convection on large-scale flow. *J. Atmos. Sci. 31*, 1232–1240.

Kuo, Y.-H. and Reed, R. J. 1988. Numerical simulation of an explosively deepening cyclone in the eastern Pacific. *Mon. Wea. Rev. 116*, 2081–2105.

Leslie, L. M., Holland, G. J. and Lynch, A. H. 1987. Australian east-coast cyclones. Part II: Numerical Modeling Study. *Mon. Wea. Rev. 115*, 3037–3053.

Manabe, S., Smagorinsky, J. and Strickler, R. F. 1965. Simulated climatology of a general circulation model with a hydrologic cycle. *Mon. Wea. Rev. 93*, 769–797.

Nordeng, T. E. 1986. Parameterization of physical processes in a three dimensional numerical weather prediction model. *Tech. Rep. No. 65*, The Norwegian Meteorological Institute, Oslo, Norway, 61 pp.

Nordeng, T. E. 1987. The effect of vertical and slantwise convection on the simulation of polar lows. *Tellus 39A*, 354–375.

Økland, H. 1987. Heating by organized convection as a source of polar low intensification. *Tellus 39A*, 397–407.

Rasmussen, E. and Zick, C. 1987. A subsynoptic vortex over the Mediterranean with some resemblance to polar lows. *Tellus 39A*, 408–425.

Reed, R. J. and Duncan, C. N. 1987. Baroclinic instability as a mechanism for the serial development of polar lows: a case study. *Tellus 39A*, 376–384.

Sanders, F. and Bosart, L. F. 1985. Mesoscale structure in the Megalopolitan Snowstorm of 11–12 February 1983. Part I: Frontogenetical forcing and symmetric instability. *J. Atmos. Sci. 42*, 1050–1061.

Sardie, J. M. and Warner, T. T. 1985. A numerical study of the development mechanism of polar lows. *Tellus 37A*, 460–477.

Sawyer, J. S. 1956. The vertical circulation at meteorological fronts and its relation to frontogenesis. *Proc. Roy. Soc. A234*, 246–262.

Sundqvist, H. 1988. Parameterization of condensation and associated clouds in models for weather prediction and general circulation simulation. In: *Physically-based modelling and simulation of climate and climatic change* (ed. M. E. Schlesinger). Dordrecht: Reidel, 433–461.

Sundqvist, H., Berge, E. and Kristjánsson, J. E. 1989. Cloud parameterization studies with a mesoscale NWP model. *Mon. Wea. Rev. 117*, 1641–1657.

Thorpe, A. 1986. Parameterization of mesoscale processes. Proceedings, Volume 1. *Seminar on Physical parameterization for numerical models of the atmosphere.* ECMWF, Reading, UK, 205–232.

Tiedtke, M., Geleyn, J.-F., Hollingsworth, A. and Louis, J.-F. 1979. ECMWF model-parameterization of sub-grid scale processes. *Tech. Rep. No. 10.* ECMWF, Reading, UK, 45 pp.

Zhang, D.-L. and Fritsch, J. M. 1986. Numerical simulation of the meso-β scale structure and evolution of the 1977 Johnstown flood. Part I: Model description and verification. *J. Atmos. Sci. 43*, 1913–1943.